Improving the performances of a high Tc superconducting circular microstrip antenna with multilayered configuration and anisotropic dielectrics

Fadila Benmeddour, Christophe Dumond, F. Benabdelaziz, F. Bouttout

Progress In Electromagnetics Research C, Vol. 18, 169–183, 2011

IMPROVING THE PERFORMANCES OF A HIGH T_C SUPERCONDUCTING CIRCULAR MICROSTRIP ANTENNA WITH MULTILAYERED CONFIGURATION AND ANISOTROPIC DIELECTRICS

F. Benmeddour

Electronics Departement
University of M'sila, M'sila 28000, Algeria

C. Dumond

PRISME Institut, IUT of Chartres
University of Orléans, France

F. Benabdelaziz

Electronics Departement
University of Constantine, Constantine 25000, Algeria

F. Bouttout

Electronics Departement
University of M'sila, M'sila 28000, Algeria

Abstract—The moment method technique has been improved to investigate the scattering properties of high T_c superconducting circular antennas with anisotropic substrate in multi-layered configuration. In this method, the electric field integral equation for a current element on a grounded dielectric slab of infinite extent was developed by basis functions involving Chebyshev polynomials. An improved analytical model is presented taking into account anisotropic substrate, superconducting material for the circular patch and multilayered structure. To validate the theoretical results, an experimental study has been performed for a perfectly conducting circular patch on a single layer, with and without air gap. Good agreements were obtained between our theory and measurements. Effects of temperature and thickness

Received 27 October 2010, Accepted 6 December 2010, Scheduled 13 December 2010
Corresponding author: Fadila Benmeddour (benmeddourfadila@yahoo.fr).

of a superconducting film are also reported and discussed. The performances of high T_c superconducting circular antennas were improved by the use of uniaxial anisotropy substrate and multilayer configuration.

1. INTRODUCTION

A superconducting antenna was one of the first microwave components to be demonstrated as an application of high-temperature superconducting material [1]. Since then, there has been considerable work on new types of superconducting antennas, with patch antennas looking like an interesting possibility for a number of applications [2].

Superconducting or perfect microstrip antennas are becoming popular and getting increased attention in both theoretical research and engineering applications due to their excellent advantages [2–6]. They are characterized by their low profile, small size, light weight, low cost and ease of fabrication, which makes them very suitable for microwave and millimeter-wave device applications [7]. They are also compatible with wireless integrated communication.

However, microstrip antennas have the limitations of narrow bandwidth, low gain and poor efficiency. Efficiency can be improved by the use of superconducting patch [8, 9]. Nevertheless, these investigations which include the rectangular, circular and annular patch, have found that the superconducting microstrip antenna suffers from inherently narrow bandwidth. To minimize this problem, anisotropic substrate and multilayered structure (air gap tuned structure) are proposed in this work.

Several methods exist for the analysis of microstrip antennas. These methods can be classified as the approximate and the full-wave methods. Some of the popular approximate models include: the transmission-line model, the cavity model and the segmentation model. These models usually consider the microstrip patch as a transmission line or a cavity resonator. Three very popular full wave methods that can be used to characterise microstrip patch antennas are: the finite element method, the finite difference time domain method, and the moment method [3]. The last one is arguably the most popular [4–6] and will be used in our work. For that, a rigorous full-wave analysis with basis modes involving Chebyshev polynomials is developed and applied.

2. THEORY

Figure 1 shows the high T_c superconducting microstrip antenna configuration. The patch is circular with radius a and thickness t. The

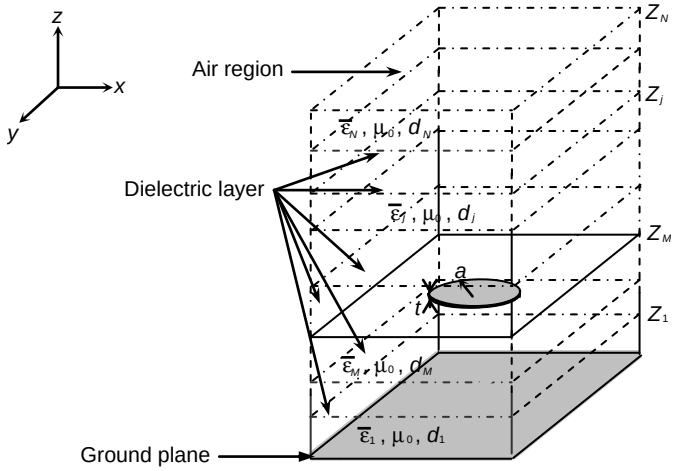

Figure 1. Superconducting circular microstrip antenna with multilayered configuration and anisotropic dielectrics.

layers of the substrate are taken to be infinite in extent and these layers are also assumed to be made of the uniaxial anisotropic dielectrics, characterized by a permittivity tensor given by [4, 5]:

$$\bar{\varepsilon}_j = \varepsilon_0 \begin{vmatrix} \varepsilon_{jx} & 0 & 0 \\ 0 & \varepsilon_{jy} & 0 \\ 0 & 0 & \varepsilon_{jz} \end{vmatrix} \tag{1}$$

where $\varepsilon_{jx} = \varepsilon_{jy} \neq \varepsilon_{jz}$, and j: number of layers

The permeability of the anisotropic dielectrics will be taken as μ_0 (the free-space permeability).

The transverse field components in the jth layer can be obtained using the vector Hankel transform formulation [4, 10].

$$E(r) = E(\rho, \phi, Z) = \begin{bmatrix} E_\rho(r) \\ H_\varphi(r) \end{bmatrix} = \sum_{n=-\infty}^{\infty} e^{in\varphi} \int_0^\infty dk_\rho k_\rho \bar{\mathbf{H}}_n(k_\rho \rho).\mathbf{e}_n(k_\rho, Z_j) \tag{2}$$

$$H(r) = H(\rho, \phi, Z) = \begin{bmatrix} -H_\varphi(r) \\ H_\rho(r) \end{bmatrix} = \sum_{n=-\infty}^{\infty} e^{in\varphi} \int_0^\infty dk_\rho k_\rho \bar{\mathbf{H}}_n(k_\rho \rho).\mathbf{h}_n(k_\rho, Z_j) \tag{3}$$

k_ρ is the spectral variable. $\bar{\mathbf{H}}_n(k_\rho \rho)$ is the kernel of the vector Hankel transform given by [11].

$$\bar{\mathbf{H}}_n(k_\rho \rho) = \begin{bmatrix} \dot{J}_n(k_\rho \rho) & \frac{-in}{k_\rho \rho} J_n(k_\rho \rho) \\ \frac{in}{k_\rho \rho} J_n(k_\rho \rho) & \dot{J}_n(k_\rho \rho) \end{bmatrix}$$

$J_n(k_\rho\rho)$ are Bessel function of the first kind of order n.

Let the generalized multilayer circular antenna represented in Figure 1, be considered. It consists of N dielectric slabs of thickness $d_j = z_j - z_{j-1}$. The circular disk is embedded in the stratification at the interface plane $z = z_M$.

The expression of the spectral dyadic Green function of the stratified medium, in which the patch is embedded, is shown to be given by [4, 10]:

$$\begin{aligned}\bar{\mathbf{G}}(k_\rho) &= \mathrm{diag}[G^{\mathrm{TM}}, G^{\mathrm{TE}}] \\ &= -(\bar{\Gamma}_<)_{12} \cdot [\bar{\mathbf{g}}_0 \cdot (\bar{\Gamma}_>)_{12} - (\bar{\Gamma}_>)_{22}] \cdot [\bar{\mathbf{g}}_0 \cdot (\bar{\Gamma})_{12} - (\bar{\Gamma})_{22}]^{-1} \quad (4)\end{aligned}$$

where

$$\bar{\Gamma}_< = \prod_{j=M}^{1} \bar{\mathbf{T}}_j, \quad \bar{\Gamma}_> = \prod_{j=N}^{M+1} \bar{\mathbf{T}}_j, \quad \text{and} \quad \bar{\Gamma} = \bar{\Gamma}_> \cdot \bar{\Gamma}_<.$$

Here, the expression of the matrices $\bar{\mathbf{T}}_j$ for the anisotropy in the dielectrics is given by:

$$\bar{\mathbf{T}}_j = \begin{bmatrix} \cos\bar{\theta}_j & i\bar{\mathbf{g}}_j^{-1} \cdot \sin\bar{\theta}_j \\ -i\bar{\mathbf{g}}_j \cdot \sin\bar{\theta}_j & \cos\bar{\theta}_j \end{bmatrix} \quad (5)$$

where: $\bar{\theta}_j = \bar{\mathbf{k}}_{jz} d_j$.
In which

$$\bar{\mathbf{k}}_{jz} = \begin{bmatrix} k_{jz}^e & 0 \\ 0 & k_{jz}^h \end{bmatrix} = \begin{bmatrix} \left(\varepsilon_{jx}k^2 - \frac{\varepsilon_{jx}}{\varepsilon_{jz}}k_\rho^2\right)^{\frac{1}{2}} & 0 \\ 0 & \left(\varepsilon_{jx}k^2 - k_\rho^2\right)^{\frac{1}{2}} \end{bmatrix} \quad (6)$$

And

$$\bar{\mathbf{g}}_j(k_\rho) = \begin{bmatrix} \tilde{g}_j^e(k_\rho) & 0 \\ 0 & \tilde{g}_j^h(k_\rho) \end{bmatrix} = \begin{bmatrix} \frac{\omega\varepsilon_{jx}\varepsilon}{k_{jz}^h} & 0 \\ 0 & \frac{k_{jz}^e}{\omega\mu} \end{bmatrix} \quad (7)$$

$k = \omega\sqrt{\mu\varepsilon}$: is the free space wavenumber. k_{jz}^e and k_{jz}^h the TM and TE propagation constants in the uniaxial substrate.

Note that the presence of an arbitrarily number of layers above and/or below the disk is easily included in the matrix product $\bar{\Gamma}_<$ and/or $\bar{\Gamma}_>$.

In applying Galerkin method to solve the vector dual integral equations, it is advantageous to express the unknown patch current in terms of appropriate expansion modes formed expansion basis functions consisting of combinations of Chebyshev polynomials, with weighting factors of the form $[1 - (\rho/a)^2]^{\pm\frac{1}{2}}$ dictated by physical constraints [4, 10].

The unknown currents expand as follows:

$$K_n(\rho) = \begin{cases} \sum_{p=1}^{P} a_{np}\Psi_{np}(\rho) + \sum_{q=1}^{Q} b_{nq}\Phi_{nq}(\rho) & a < \rho \\ 0 & \rho > a \end{cases} \tag{8}$$

with

$$\Psi_{np}(\rho) = \begin{cases} \begin{bmatrix} (\rho/a)^{n-2}U_{2p-1}(\rho/a)\sqrt{1-(\rho/a)^2} \\ 0 \end{bmatrix} & \rho < a \\ \mathbf{0} & \rho > a \end{cases}$$
$$n \in \mathbf{N}^*, \quad p = 1, 2, 3, \ldots, P \tag{9}$$

$$\Phi_{nq}(\rho) = \begin{cases} \begin{bmatrix} 0 \\ i(\rho/a)^{n-1}\frac{T_{2q-2}(\rho/a)}{\sqrt{1-(\rho/a)^2}} \end{bmatrix} & \rho < a \\ \mathbf{0} & \rho > a \end{cases}$$
$$n \in \mathbf{N}^*, \quad p = 1, 2, 3, \ldots, Q \tag{10}$$

where T and U in Equations (9) and (10) are, respectively, the Chebyshev polynomials of the first and second kind.

Consider the evaluation of the vector Hankel transform VHT of (9) and (10). The basis functions given in (11)–(12) are then Hankel transformed to obtain $\tilde{\Psi}_{np}$ and $\tilde{\Phi}_{nq}$, whose expressions are given by [10].

$$\tilde{\Psi}_{np}(k_\rho) = \frac{a^2}{2}\begin{bmatrix} \int_0^1 dx x^{n-1}U_{2p-1}(x)\sqrt{1-x^2}J_{n-1}(\xi x) \\ -\int_0^1 dx x^{n-1}U_{2p-1}(x)\sqrt{1-x^2}J_{n+1}(\xi x) \\ \\ i\left[\int_0^1 dx x^{n-1}U_{2p-1}(x)\sqrt{1-x^2}J_{n-1}(\xi x)\right. \\ \left. +\int_0^1 dx x^{n-1}U_{2p-1}(x)\sqrt{1-x^2}J_{n+1}(\xi x)\right] \end{bmatrix}$$
$$n \in \mathbf{N}^*, \quad p = 1, 2, 3, \ldots, P \tag{11}$$

$$\tilde{\Phi}_{nq}(k_\rho) = \frac{a^2}{2}\left[\begin{array}{l} -i\left[\int_0^1 dx x^n \frac{T_{2q-2}(x)}{\sqrt{1-x^2}} J_{n-1}(\xi x) + \int_0^1 dx x^n \frac{T_{2q-2}(x)}{\sqrt{1-x^2}} J_{n+1}(\xi x)\right] \\ \\ \int_0^1 dx x^n \frac{T_{2q-2}(x)}{\sqrt{1-x^2}} J_{n-1}(\xi x) - \int_0^1 dx x^n \frac{T_{2q-2}(x)}{\sqrt{1-x^2}} J_{n+1}(\xi x) \end{array}\right]$$

$$n \in \mathbf{N}^*, \quad q = 1, 2, 3, \ldots, Q \tag{12}$$

with: $\xi = k_\rho a$

To include the effect of the superconductivity of the microstrip antenna in full-wave analysis, surface complex impedance for a plane electromagnetic wave incident normally to its surface is defined as the ratio of $|E|$ to $|H|$ on the surface of the sample it is given by [12–14]:

$$Z_S = R_S + X_S \tag{13}$$

where R_s and X_s are the surface resistance and the surface reactance. When the thickness t of the superconducting patch is less than three times the penetration depth λ_0 at a temperature $T = 0\,\mathrm{K}$ the surface impedance can be approximated as follows:

$$Z_S = \frac{1}{t\sigma} \tag{14}$$

where the conductivity σ is real for conventional conductors, these approximations have been verified for practical metallization thicknesses in comparison to rigorous mode matching results. The complex conductivity σ of the superconducting film is determined by using London's equation and the model of Gorter and Gasimir as [9]:

$$\sigma = \sigma_1 - i\sigma_2 \tag{15}$$

σ_1 may arise from normal electron conduction within non superconducting grains and scattering from grain boundaries, flux vibration at pinning centers and normal electron conduction due to thermal agitation in the superconducting state. The reactive part of the conductivity $(-i\sigma_2)$ arises from the lossless motion of the superconducting carries which may be derived from the Lorentz-force equation as [12–14]:

$$\sigma_1 = \sigma_n (T/T_c)^4 \quad \text{and} \quad \sigma_2 = \frac{1 - (T/T_c)^4}{\omega \mu_0 \lambda_0^2} \tag{16}$$

where

σ_n: is often associated with the normal state conductivity at the transition temperature of the superconductor T_c.

ω: is the angular frequency.

The concept of calculating the resonant frequency is embodied in the following set of vector dual integral equations:

$$\mathbf{e}_n(\rho) = \int_0^\infty dk_\rho k_\rho \bar{\mathbf{H}}_n(k_\rho\rho) \cdot (\bar{\mathbf{G}}(k_\rho) - \bar{Z}_S) \cdot \mathbf{K}_n(k_\rho) = \mathbf{0} \quad \rho < a \tag{17}$$

$$\kappa_n(\rho) = \int_0^\infty dk_\rho k_\rho \bar{\mathbf{H}}_n(k_\rho\rho) \cdot \mathbf{K}_n(k_\rho) = \mathbf{0} \quad \rho > a \tag{18}$$

where

$$\bar{Z}_S = \begin{vmatrix} Z_s & 0 \\ 0 & Z_s \end{vmatrix} \tag{19}$$

The electric field integral equation which enforces the boundary condition must vanish on the patch surface, as discretized into a matrix form shown as:

$$\begin{bmatrix} \bar{\mathbf{Z}}'^{\psi\psi})_{M\times M} & (\bar{\mathbf{Z}}'^{\psi\varphi})_{M\times P} \\ (\bar{\mathbf{Z}}'^{\varphi\psi})_{P\times M} & (\bar{\mathbf{Z}}'^{\varphi\varphi})_{P\times P} \end{bmatrix} \cdot \begin{bmatrix} (\mathbf{A}')_{M\times 1} \\ (\mathbf{B}')_{P\times 1} \end{bmatrix} = \mathbf{0} \tag{20}$$

Each element of the submatrices $\bar{Z}'^{CD}_{ij}$ is given by:

$$\bar{Z}'^{CD}_{ij} = \int_0^\infty dk_\rho k_\rho \mathbf{C}^+_{ni}(k_\rho) \cdot (\mathbf{G}(k_\rho) - \bar{Z}_S) \cdot \mathbf{D}_{nj}(k_\rho) \tag{21}$$

where C and D represent either φ or ψ for every value of the integer n.

The system of linear equation has non-trivial solutions when the determinant of system Equation (20) vanishes, that is:

$$\det([\bar{Z}'(f)]) = 0 \tag{22}$$

Equation (22) is the characteristic equation for the complex resonant frequency: $f = f_r + if_i$, where f_r is the resonant frequency, and $BW = 2f_i/f_r$ is the half-power fractional bandwidth of the antenna [4].

3. RESULTS AND DISCUSSION

3.1. Validation of Results for a Perfect Conducting Circular Patch Microstrip Antenna

The aim in this section is to valid the results. The considered structure is a circular microstrip antenna with a single isotropic layer ($j = 1$). In

Table 1. Comparison of measured and calculated resonant frequencies for different disk radius a. $\varepsilon_{1x} = \varepsilon_{1z} = 2.43$, $d_1 = 0.49\,\text{mm}$.

a/d_1	Results [4]			Our results	
	fr (GHz) Mesured	fr (GHz) Calculated	$\Delta fr^{\text{ex-nu}}$	fr (GHz)	$\Delta fr^{\text{ex-nu}}$
4.02	25.6	25.3	+1.2%	25.92	−1.2%
8.08	13.1	13.3	−1.5%	13.55	−3.4%
12.02	8.96	9.13	−1.9%	9.25	−3.2%
16.33	6.81	6.80	+ 0.2%	6.87	−1%
20.33	5.47	5.49	−0.4%	5.54	−1.2%

Table 2. Comparison of measured and calculated resonant frequencies for a single isotropic layer $d_1 = 1.57\,\text{mm}$, $\varepsilon_{1x} = \varepsilon_{1z} = 2.05$, and $\text{tg}(\delta) = 0.00045$.

a (mm)	fr (GHz) (MoM Chebyshev polynomials)	fr (GHz) Our measurements results
10	5.589	5.63
15	3.825	3.81
20	2.909	2.92

order to make a validation, we have first compared our results with the theoretical and experimental results of Losada et al. [4]. The perfectly conducting circular antenna is printed on a substrate of permittivity $\varepsilon_{1x} = \varepsilon_{1z} = 2.43$, with a thickness $d_1 = 0.49\,\text{mm}$. The Table 1 summarizes our computed resonant frequencies and those obtained for TM_{11} mode via formulation of Losada et al. [4]. The comparisons show a good agreement between our results and those of literature.

To complete this validation, experimentations have been performed at the PRISME institute of University of Orleans. An Agilent E5071B vector network analyser has been used for measurements. The perfect conducting circular disk microstrip antennas were fabricated using printed circuit processing techniques and were alimented by coax-feed.

In Table 2, we compare our theoretical values of resonant frequencies by using the full-wave moment method (MoM), with our experimental results. The antennas with perfectly conducting patch for three different radius a, and substrates are fabricated on Cuflon material with $\varepsilon_{1x} = \varepsilon_{1z} = 2.05$ and thickness $d_1 = 1.57\,\text{mm}$. A good

agreement is obtained between measurements and theoretical results.

An adjustable air gap will be proposed and studied in the following section to improve the bandwidth of the structure. In this way, a perfectly conducting patch, with a RT/Duroid 5870 substrate of $\varepsilon_{2x} = \varepsilon_{2z} = 2.32$, $d_2 = 1.5748\,\text{mm}$ and $\text{tg}\delta = 0.0014$, has been realized and measured with different air gap thickness. Measured and calculated resonant frequencies and bandwidths are listed in Table 3. Results show an important increase of the bandwidth with the air separation. Again, acceptable agreements were obtained.

Table 3. Comparison of measured and calculated frequencies for a circular microstrip patch with different thickness of air gap d_1, $a = 50\,\text{mm}$, $\varepsilon_{2x} = \varepsilon_{2z} = 2.32$, $d_2 = 1.5748\,\text{mm}$.

d_1 (mm)	Our theorical results MoM		Our measurements results	
	fr (GHz)	$BW\%$	fr (GHz)	$BW\%$
0.5	1.272	1.457	1.262	1.632
1	1.339	1.954	1.3687	2.018
2	1.398	2.911	1.462	3.122
3	1.417	3.848	1.5	4.208
4	1.420	4.778	1.53	4.5

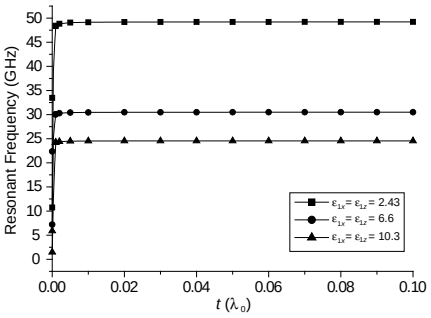

Figure 2. The resonant frequency versus the thickness of patch ($\sigma_n = 210\,\text{s/mm}$, $\lambda_0 = 1500\,\text{Å}$ and $T/T_c = 0.5$, $a = 1\,\text{mm}$, $d_1 = 1.2\text{mm}$).

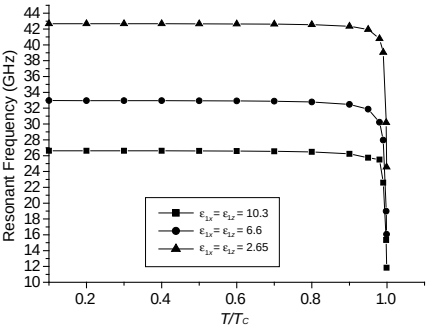

Figure 3. The resonant frequency versus the normalized temperature ($\sigma_n = 210\,\text{s/mm}$, $\lambda_0 = 1500\,\text{Å}$ and $t_c = 89°$, $a = 1\,\text{mm}$, $d_1 = 1.2\,\text{mm}$ and $t = 0.02\,\mu\text{m}$).

3.2. Resonant Frequency of Superconducting Circular Patch Antenna

In high frequencies when dimensions of the antennas become very small compared to the free space wavelength, recent studies have found that high losses occur [2, 6, 8, 13]. In order to reduce them, the use of high T_c superconducting material for the patch has been proposed. In this study the influences of the thickness of superconducting film t and of the normalized temperature (T/T_c) of the antenna are considered for three different relative permittivity of substrate $\varepsilon_{1x} = \varepsilon_{1z} = 2.43$, $\varepsilon_{1x} = \varepsilon_{1z} = 6.6$ and $\varepsilon_{1x} = \varepsilon_{1z} = 10.33$. The superconducting material YBCO which has been used for the simulation is characterized by: $\sigma_n = 210\,\mathrm{s/mm}$, $\lambda_0 = 1500\,\text{Å}$ and $T_c = 89\,\mathrm{K}$. In Figure 2, it is observed that as the thickness of superconductor patch grows, the resonant frequency increases quickly until the thickness t reaches λ_0 (penetration depth). After this value, increasing the superconducting thickness will increase slowly the resonance frequency. Also it can be observed that increasing the temperature will decrease gradually the resonant frequency. In Figure 3 this decrease is more significant for temperature values near the critical temperature T_c. These behaviors agree with those reported by Richard et al. [13].

The bandwidth of high T_c superconducting disk antennas around

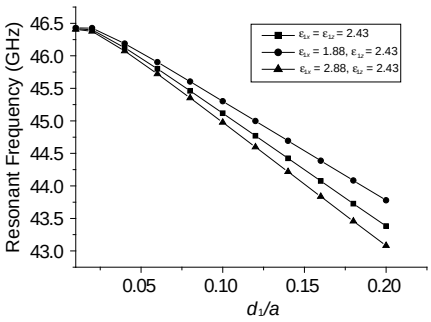

Figure 4. Resonant frequency versus the substrate thickness for: Isotropic ($\varepsilon_{1x} = \varepsilon_{1z} = 2.43$); positive uniaxial ($\varepsilon_{1x} = 1.88$, $\varepsilon_{1z} = 2.43$), negative uniaxial ($\varepsilon_{1x} = 2.88$, $\varepsilon_{1z} = 2.43$), $T/T_c = 0.5$, $t = 0.15\,\mu\mathrm{m}$, $\sigma = 210\,\mathrm{s/mm}$, $\lambda_0 = 1500\,\text{Å}$, $a = 1.5\,\mathrm{mm}$.

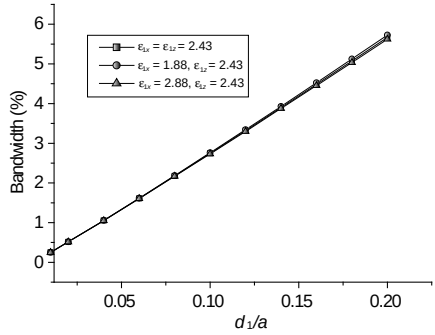

Figure 5. Bandwidth versus the substrate thickness for: Isotropic ($\varepsilon_{1x} = \varepsilon_{1z} = 2.43$); positive uniaxial ($\varepsilon_{1x} = 1.88$, $\varepsilon_{1z} = 2.43$), negative uniaxial ($\varepsilon_{1x} = 2.88$, $\varepsilon_{1z} = 2.43$), $T/T_c = 0.5$, $t = 0.15\,\mu\mathrm{m}$, $\sigma = 210\,\mathrm{s/mm}$, $\lambda_0 = 1500\,\text{Å}$, $a = 1.5\,\mathrm{mm}$.

their operating resonant frequencies is known to be very narrow. In order to improve it, we propose in Sections 3-3 and 3-4, two structures.

3.3. Superconducting Circular Patch Antenna in Presence of Anisotropic Uniaxial Substrate

In order to study the effect of anisotropic substrate on superconducting patch antenna, the resonant frequency has been calculated for different pairs of relative permittivity $(\varepsilon_{1x}, \varepsilon_{1z})$. The same YBCO material characteristics have been considered.

The results are plotted in Figures 4, 5, 6 and 7. Whereas the antenna parameters (resonance frequency, bandwidth) do not vary significantly with the permittivity variation perpendicular to the optical axis (ε_{1x}), these are found to be strongly dependent with the permittivity variation along the optical axis (ε_{1z}).

Interesting enhancement of the bandwidth is obtained for the case of negative uniaxial anisotropy along the optical axis.

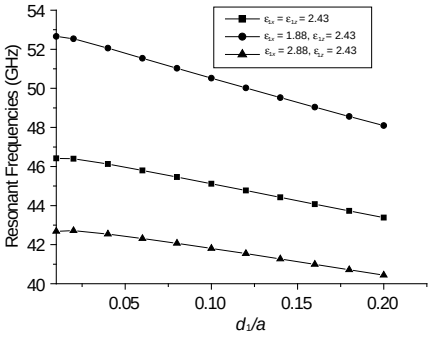

Figure 6. Resonant frequency versus the substrate thickness for: Isotropic ($\varepsilon_{1x} = \varepsilon_{1z} = 2.43$); positive uniaxial ($\varepsilon_{1x} = 2.43$, $\varepsilon_{1z} = 2.88$); and negative uniaxial ($\varepsilon_{1x} = 2.43$, $\varepsilon_{1z} = 1.88$), $T/T_c = 0.5$, $t = 0.15\,\mu$m, $\sigma = 210\,$s/mm, $\lambda_0 = 1500\,$Å, $a = 1.5\,$mm.

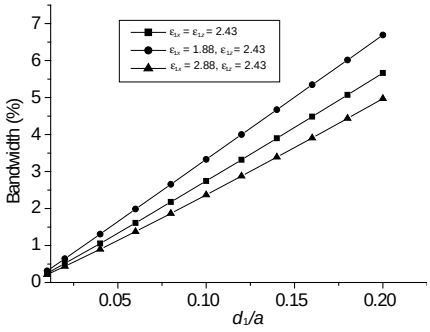

Figure 7. Bandwidth versus the substrate thickness for: Isotropic ($\varepsilon_{1x} = \varepsilon_{1z} = 2.43$); positive uniaxial ($\varepsilon_{1x} = 2.43$, $\varepsilon_{1z} = 2.88$); and negative uniaxial ($\varepsilon_{1x} = 2.43$, $\varepsilon_{1z} = 1.88$), $T/T_c = 0.5$, $t = 0.15\,\mu$m, $\sigma = 210\,$s/mm, $\lambda_0 = 1500\,$Å, $a = 1.5\,$mm.

3.4. Superconducting Circular Patch Antenna in Multilayered Configuration

In order to achieve tunable resonant frequency and improve the bandwidth, an adjustable air gap layer can be inserted between the ground plane and the substrate, resulting in a two layer structure ($j = 2$). These structures, first introduced by Dahel and Lee [15, 18], have been investigated by the cavity model without the superconductor material. They have received a great deal of attention in recent years [16, 17, 19].

Here the effect of an air gap on the resonant frequency and bandwidth of a circular high T_c superconducting microstrip antenna versus the air separation for various substrate materials have been computed using our numerical method. Results are shown in Figures 8 and 9.

Again the structure of the same superconducting YBCO thin film has been simulated. Figure 8 shows that an increase in the air separation, results in a fast increase of the resonance frequency until it reaches a maximum. Note that the effect of the air gap is more pronounced for small values of d_1. Moreover, an important increase in the resulting bandwidth is also obtained in Figure 9.

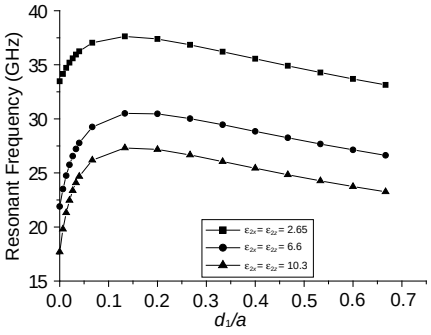

Figure 8. Resonant frequency versus the air separation, for circular microstrip antenna for three dielectric constant: $\varepsilon_{2x} = \varepsilon_{2z} = 2.65$, $\varepsilon_{2x} = \varepsilon_{2z} = 6.6$, and $\varepsilon_{2x} = \varepsilon_{2z} = 10.3$, $a = 1.5\,\text{mm}$. $\sigma_n = 210\,\text{s/mm}$, $\lambda_0 = 1500\,\text{Å}$, and $T/T_c = 0.5$, and $t = 0.02\,\mu\text{m}$.

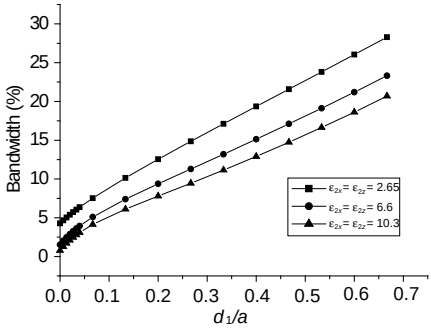

Figure 9. Bandwidth versus the air separation, for circular microstrip antenna for three dielectric constant: $\varepsilon_{2x} = \varepsilon_{2z} = 2.65$, $\varepsilon_{2x} = \varepsilon_{2z} = 6.6$, and $\varepsilon_{2x} = \varepsilon_{2z} = 10.3$, $a = 1.5\,\text{mm}$. $\sigma_n = 210\,\text{s/mm}$, $\lambda_0 = 1500\,\text{Å}$, and $T/T_c = 0.5$, and $t = 0.02\,\mu\text{m}$.

4. CONCLUSION

Our studies investigated the multilayer substrate and the effects of anisotropic substrate on the performance of high T_c superconducting circular microstrip patch. The numerical method used is based on spectral method and the integral equation formulation developed using the basis functions involving Chebyshev polynomials. It has been confirmed by experimental results for perfect conducting disk case.

In order to introduce the effect of a superconductor microstrip patch the surface complex impedance has been considered. Results show that the superconductor patch thickness and the temperature have significant effect on the resonant frequency of the antenna.

The effect of anisotropic substrate shows that resonance frequency and the bandwidth of a superconducting circular patch are not sensitive to a permittivity variation perpendicular to the optical axis (ε_{1x}), but are strongly affected by a permittivity variation along the optical axis (ε_{1z}). Interesting improvement of the bandwidth is obtained for the negative uniaxial anisotropy along this axis.

Moreover, the superconducting circular patch has been studied in a two layers configuration with an adjustable air gap. Results show an important augmentation of the antenna's bandwidth as the thickness of air gap increases.

REFERENCES

1. Khamas, S. K., M. J. Mehler, T. S. M. Maclean, C. E. Gough, and N. M. Alford, "High-T_c superconducting short dipole antenna," *Electronics Letters*, Vol. 24, 460–461, 1988.
2. Nisenoff, M. and J. Pond, "Superconductors and microwaves," *Microwave Magazine*, 10.1109/MMM.2009.932077, 2009.
3. Kumar, G., *Broadband Microstrip Antennas*, Artech House, Boston, London, 2003, ISBN: 1-58053-244-6.
4. Losada, V., R. R. Boix, and M. Horno, "Resonant modes of circular micristrip patches in multilayered substrates," *IEEE Transactions on Microwave Theory and Techniques*, Vol. 47, No. 10, 488–498, 2000.
5. Bouttout, F., F. Benabdelaziz, A. Benghalia, D. Khedrouche, and T. Fortaki, "Uniaxialy anisotropic substrate effects on resonance of rectangular microstrip patch antenna," *Electronics Letters*, Vol. 35, No. 4, 255–256, 1999.
6. Barkat, O. and A. Benghalia, "Synthesis of superconducting circular antennas placed on circular array using a particle

swarm optimisation and the full-wave method," *Progress In Electromagnetics Research B*, Vol. 22, 103–119, 2010.

7. Pozar, D. M., "Considerations for millimeter wave printed antennas," *IEEE Transactions on Antennas and Propagation*, Vol. 31, 740–747, 1983.
8. Hansen, R. C., *Electrically Small, Superdirective, and Superconducting Antennas*, John Wiley & Sons, Inc., Hoboken, New Jersey, 2006.
9. Chebbara, F., S. Benkouda, and T. Fortaki, "Fourier transform domain analysis of high T_c superconducting rectangular microstrip patch over ground plane with rectangular aperture," *Journal of Infrared, Millimeter, and Terahertz Waves*, Vol. 31, Nos. 881–832, Springer, 2010.
10. Benmeddour, F., F. Benabdelaziz, F. Bouttout, and N. Aouabdia, "Resonance characteristics of circular microstrip antennas using moment method and various current representations," *First International Symposium on Control, Communications and Signal Processing*, 10.1109/ISCCSP.2004.1296296, 339–342, 2004.
11. Chew, W. C. and J. A. Kong, "Resonance of non axial symmetric modes in circular micro strip disk," *Mathematical Physics*, Vol. 21, No. 10, 590–2598, 1980.
12. Nghiem, D., J. T. Williams, and D. R. Jackson, "A general analysis of propagation along multiple-layer superconducting stripline and microstrip transmission lines," *IEEE Transactions Microwave Theory and Techniques*, Vol. 39, No. 9, 1553–1565, 1991.
13. Richard, M. A., K. B. Bhasin, and P. C. Claspy, "Superconducting microstrip antennas: An experimental comparison of two feeding methods," *IEEE Transactions on Antennas and Propagation*, Vol. 41, No. 7, 967–974, 1993.
14. How, H., R. G. Seed, C. Vittoria, D. B. Chrisey, J. S. Horwitz, C. Carosella, and V. Folen, "Microwave characteristics of high T_c superconducting coplanar waveguide resonator," *IEEE Transactions on Microwave Theory and Techniques*, Vol. 40, No. 8, 1668–1673, 1992.
15. Lee, K. F., K. Yho, and J. S. Dahel, "Circular-disk microstrip antenna with an air gap," *IEEE Transactions on Antennas and Propagation*, Vol. 32, No. 8, 1984.
16. Guha, D., "Resonant frequency of circular microstrip antennas with and without air gaps," *IEEE Transactions on Antennas and Propagation*, Vol. 49, No. 1, 2001.

17. Gürel, Ç. S., E. Aydın, and E. Yazgan, "Computation and optimisation of resonant frequency and input impedance of coax-fed circular patch microstrip antenna," *Microwave and Optical Technology Letters*, Vol. 49, No. 9, 2007.
18. Dahel, J. S. and K. F. Lee, "Theory and experiment on microstrip antenna with air-gap," *IEEE Proceeding*, Vol. 132, No. 7, 455–460, 1985.
19. Fortaki, T., S. Benkouda, M. Amir, and A. Benghalia, "Air gap tuning effect on the resonant frequency and half-power bandwidth of superconducting microstrip patch," *PIERS Online*, Vol. 5, No. 4, 350–354, 2009.